*Journal of Multidisciplinary Modeling and Optimization 4(1) (2021), 19-31.*

# Identification of Material Using Muography

Muhanad ALYASIRI

[1]Department of Physics, Faculty of Arts and Sciences,
Suleyman Demirel University, Isparta, Turkey
muhanadshamar@gmail.com
*ORCID: https://orcid.org/0000-0002-2670-5418*

Received: 13.07.2021, Accepted: 27.12.2021, Published: 03.01.2022

**Abstract** — *Muography is an imaging technique based on the absorption or scattering of atmospheric muons produced from cosmic-ray interactions in the atmosphere. These muons are abundant at sea level and thus provide a natural source for imaging. Scattering density is a characteristic of matter that can be used to discriminate between different materials. When muons pass through material they produce an aggregate of scattering angles with an approximately Gaussian distribution. The standard deviation of the distribution can be calculated using the radiation length of the substance. In this study, we calculated the scattering densities for 20 elements at different four values of the momentum of the muons to show the dependency on the momentum of the incident muons. Our results presented in this study complete the results obtained in some previous related studies.*

**Keywords:** Cosmic rays, Muography, Material identification.

## 1 Introduction

Cosmic rays are a natural source of high-energy particles. The study of cosmic radiation remains, even today, fundamental for both subnuclear physics and astrophysics. We know rather well the energy spectrum of cosmic rays. It extends up to $100EeV$ ($10^{20}eV$). At these extreme energies the flux is very low, typically one particle per square kilometer per century. To make a comparison, notice that the highest-energy accelerator, the LHC at CERN, has a center of mass energy of (14 TeV), corresponding to only (0.1 EeV)[1]. Protons or nuclei, which are among the components of cosmic rays, penetrate the atmosphere of the earth and collide with nuclei of the air. This strong interaction produces pion, less frequently kaon mesons and, even more rarely, other hadrons. The produced charged pions have a lifetime of only 26 ns. Thus, the negatively (positively) charged pions quickly decay into muons (anti-muons) and muon anti-neutrions (neutrinos)[2, 3].

Muon is considered from elementary subatomic particle similar to electron but 207 times heavier than electron. Muon was discovered as a constituent of cosmic-ray particle ”showers” in 1936. Because of its mass, it was thought to be particle predicted by

Japanese physicist Yukawa Hideki in 1935 to explain the strong force that binds protons and neutrons together in atomic nuclei[2, 3]. A muon is relatively unstable, with a lifetime of only $2.2\,\mu s$ before it decays by the weak force into an electron and two kinds of neutrinos. Since muons are charged particles, before decaying, they lose energy by displacing electrons from atoms through ionization process. At velocities close to the speed of light, ionization dissipates energy in relatively small amounts, so muons in cosmic radiation are extremely penetrating and thus can travel to some distances below earth surface.The interest in the use of muons for imaging issues in the field of Earth Sciences, as said before, emerged soon after the discovery of these particles and their properties. Muons found in cosmic rays can go through hundreds of meters (the most energetics also through kilometers) of rock, undergoing attenuations related to the quantity of matter traversed [4]. Initially, the muons imaging technique was born from the need to characterize from a geological point of view the structures in the underground labs that hosted particle detectors. Subsequently, when the devices used to carry out these measurements became more portables, also measurements of geological structures such as mines, mountains, and volcanoes were conducted, with the aim of monitoring natural phenomena such as earthquakes or eruptions. The first idea to exploit the muon physical characteristics was, therefore, to use the information on the absorption of muons to measure the thickness of the material traversed by cosmic rays. The first application of cosmic rays to inspect large volumes was performed in 1955 when the thickness of a layer of rock overlying an underground tunnel was measured by E.P. George [5]. An application much more spectacular was conceived by the Nobel Prize in physics LW Alvarez [6] in 1970, in which he made radiography of the pyramid of Khafre, in order to look for hidden chambers. Recently, the same technique was used to inspect the interior of volcanoes. The operating principle is the same as the X-ray radiography. The measured quantity is the flux attenuation of the muon that crosses the target under the study. Based on this, the quantity of material encountered by muons along their trajectory can be estimated. The interaction of the muons flux with the target depends on both the size of the target and its density: thus for a small size and a low density only a few muons will interact, while a body of a large size or s dense body, most of the striking muons will be absorbed.

Though there are previous studies on the interaction of muon with materials, applications have emerged in various fields. Driven by the deep penetrating power of muons and the non-destructive feature of muography as an imaging technique, many proposals exist for using this technique in several fields. Among these fields, one can mention volcanology, archeology, security, nuclear reactor and waste imaging, underground measurements, civil engineering and material identification.

## 2 PRINCIPLES OF MUOGRAPHY TECHNIQUE

Muon reaction with matter in range (1-1000 GeV) , where be two interaction ways : Energy loss through electromagnetic interaction with electrons causing ionization, and deflection via Coulomb's multiple scattering. The distribution of scattering angles is well approximated by the Gaussian distribution[9]:

$$f_{\theta_x}(\theta_x) = \frac{1}{\sqrt{2\pi}\sigma_\theta} \exp(-\frac{\theta_x^2}{2\sigma_\theta^2}) \tag{1}$$

Where $\sigma_\theta$ is the Root Mean Square (RMS) width of the angular distribution. Therefore one can determine the density and the atomic number of the object of interest by the measurement of the scattering angles of the particles which penetrate the object and given by the following equation[7]:

$$\sigma_\theta = \frac{13.6}{p\beta c} z \sqrt{\frac{L}{L_{rad}}} [1 + 0.038 \ln(\frac{L}{L_{rad}})] \tag{2}$$

Where p is the momentum, and ($\beta c = 1$ for muons) is the velocity of the incident particle, L is the depth of the material, z atomic number and $L_{rad}$ is the radiation length of the material. Represent radiation length of material is mean length to reduce from the energy of an electron by factor 1/e. which will be affected the electron when arriving in the vicinity of an atom, where electrons will emit photons' which will reduce energy depend on the number of electrons of the atom and also on the size of the atom, represented by its atomic weight A[8].

$$L_{rad} = \frac{716.4}{Z(Z+1)\ln\frac{287}{\sqrt{Z}}}\ g.cm^{-3} \tag{3}$$

If we have a composite material with number of different materials, we can also estimate the combined radiation length of the sample.The general formula for the radiation length is then given as[8]:

$$\frac{W_o}{L_o} = \sum \frac{W_i}{L_i} \tag{4}$$

where $W_o$ is the total mass of the sample in g,$L_o$ is the combined radiation length of the sample in $gcm^2$,$W_i$ is the mass of the individual component in g and $L_i$ is the radiation length of the individual component in $gcm^2$.

The aim of multiple scattering theory is to predict $\sigma_\theta$ given with scattering material, thickness, and incident particle energy. In this theory, Moliere derived an accurate formula for single scattering in the screened Coulomb field of nucleus and also through using that formula he computed multiple scattering.

Moliere's approach to describe multiple scattering of fast charged particles is based on his theory of the single scattering process (each scattering of a particle off one atom is regarded as an independent on other scattering). It is shown that the scattering depends only on the atomic screening; the critical angle $\chi_a$ [12]. Assuming that all scattering angles are small i.e. $sin\theta \simeq \theta$ and the scattering problem is equivalent to diffusion in the plane of $\theta$, the number of charged particles in the angular interval $d\theta$ after passing a thickness t is $f(\theta, t)\theta d\theta$. Here, $f(\theta, t)$ can be calculated as [7, 8, 11]:

$$f(\theta, t) = \int_0^\infty \eta d\eta J_o(\eta\theta) \times \exp[-Nt \int_0^\infty \sigma(x) x dx \{1 - J_o(\eta x)\}] \tag{5}$$

Where $N$ is the number of scattering atoms per $cm^3$,$t$ is thickness material, $\theta$ is the scattering angle, $\sigma(x)\, x\, dx$ is the differential scattering cross section into the angular interval $dx$ and $J_o$ Bessel transformation. The scattering from atoms is characterized by the fact that $\sigma$ decreases and it is complicated only for angles of the order of:

$$\chi_o = \frac{\bar{\lambda}}{a} = \frac{\bar{\lambda}}{(0.885 a_o Z^{-\frac{1}{2}})} \tag{6}$$

Where $\bar{\lambda}$ is the de Broglie wavelength of the electron, $a_o$ the Bohr radius, and $a$ the Fermi radius of the atom. For any reasonable foil thickness, the width of the multiple scattering distribution is very large compared with $\chi_o$.

$$Nt\sigma(x)xdx = 2\chi_c^2 xdxq(x)/x^4 \tag{7}$$

Here

$$\chi_c^2 = 4\pi Nte^4 Z(Z+1)z^2/(\rho\upsilon)^2 \quad rad^2(electrons) \tag{8}$$

$$\chi_c^2 = 4\pi Nte^4 Z^2 z^2/(\rho\upsilon)^2 \quad rad^2(heavy\, particles) \tag{9}$$

Where $p$ is the momentum and $\upsilon$ represents the velocity of the scattered particle of charge $z$. The factor $Z+1$ instead of $Z$ is to take into account the scattering by the electrons of atoms. The physical meaning of $\chi_c$ is that the total probability of single scattering through an angle greater than $\chi_c$, is exactly one.
As first suggested, in Ref. [10], Moliere's transformed equation, takes simpler form compared to equation (5) as:

$$f(\theta)\theta d\theta = \lambda d\lambda \int_0^\infty y dy J_o(\lambda y) \exp[\frac{1}{4}y^2(-b + \ln\frac{1}{4}y^2] \tag{10}$$

$$b = \ln(\chi_c/\chi_a)^2 + 1 - 2C \equiv \ln(\chi_c/\chi_a)^2 \tag{11}$$

Where $C = 0.577$ is Euler's constant, $\lambda = \theta/\chi_c$, $y = \chi_c\eta$. The important result of Moliere's theory is that the scattering is described by a single parameter; the screening angle ($\chi_a$). As can be seen from Eq.(10), the distribution function $f(\theta)$ depends on $b$ and from Eq.(11) $b$ depends on the ratio of the unit probability angle ($\chi_c$), in equation(9), that describes the foil thickness to the screening angle ($\chi_a$) which describes the scattering atom. The distribution function $f(\theta)$ is entirely independent of the shape of the differential cross section [11].
For the actual determination of the screening angle $\chi_a$ Moliere uses his own calculation of the single scattering by a Thomas-Fermi potential which does not make use of the Born approximation, the solution being accomplished by means of the Wentzel Kramers Brillouin (WKB) method, which is a method for finding approximate solutions to linear differential equations with spatially varying coefficients. It is typically used for a semiclassical calculation in quantum mechanics in which the wave function is recast as an exponential function, semiclassically expanded, and then either the amplitude or the phase is taken to be changing slow[11].

$$\chi_a = \chi_o\sqrt{(1.13 + 3.76\alpha^2)} \tag{12}$$

With $\alpha$ being the usual parameter the Born approximation, [11],

$$\alpha = zZe^2/\hbar\vartheta \tag{13}$$

For the actual determination of the screening angle ($\chi_a$)Moliere uses his own calculation" of the single scattering by a Thomas-Fermi potential which does not make use of the Born approximation.

$$\alpha = \frac{zZ}{(137\beta)} \approx \frac{1}{137} \tag{14}$$

# 3 RESULTS

In this section we present our results. We consider a target material of thickness (10 cm) in accordance with a previous study carried in 2001 where out by Christopher Morris and William Priedhorsky of Los Alamos National Laboratory (LANL) and considered as a novel form of radiography. Their idea was to make use of the multiple Coulomb scattering experienced by cosmic ray muons passing through objects to segregate materials of high and low atomic density. Morris and Priedhorsky set together a small team of researchers at LANL, including themselves. The goal of this team was to provide a proof of the principle for cosmic-ray muon radiography. To achieve this goal the team outlined four primary objectives. These objectives are building a small prototype and gather experimental data, implementing a Monte Carlo simulation of the experiment, developing an object reconstruction algorithm and producing reconstructions of experimental data (to prove the concept) and simulated data (to validate understanding)). By 2003 these objectives were achieved and documented in Ref.[16]. A new form of radiography of small objects, based on using passive cosmic ray muons, was introduced. A significant amount of press attention followed, and cosmic ray muon radiography was featured in Physics Today [17], on National Public Radio [18], and several websites, including those of National Geographic [19], Science News [20], and the BBC.

The technique exploits the multiple Coulomb scattering of muons for non-destructive inspection without the use of artificial radiation. The muon sources used in the technique were originating from cosmic rays with the typical sea-level flux. The energy of the muons were ranging between 1 GeV-10 GeV with average 3 GeV-4 GeV.

The scattering density is a characteristic of the material. It depends on the standard deviation of the distribution of scattering angles produced as a result of the scattering of muons after exiting material. We will evaluate the standard deviation using two different methods; using the radiation length $L_{rad}$ and using a simple Gaussian approximation of Moliere's theory which will be discussed in the following.

### 3.1 Materials Identification Based On Radiation Length

When charged particles cross a matter they produce aggregate of scattering angles $\theta$ and displacements from the un-scattered exit point. The angular scattering distribution is approximately Gaussian. The standard deviation of both distributions may approximately be expressed in terms of material properties as[9]

$$\sigma_\theta \cong \frac{15}{p_\circ}\sqrt{\frac{L}{L_{rad}}} \tag{15}$$

It is clear from the equation that a large depth of a lower Z (higher $L_{rad}$) material may produce a scattering equivalent to that produced by a higher Z (lower $L_{rad}$) material. Scattering is also influenced by particle momentum $p$. To identify material it is necessary to normalize for these two effects[12, 14]. Establishing a nominal muon momentum $p_o$ and squaring both sides of equation (15):

$$\sigma_\theta^2 = (\frac{15}{p_o})^2[\frac{1}{L_{rad}}]L \tag{16}$$

The scattering density of a material with radiation length $L_{rad}$ is defined as:

$$\lambda \equiv (\frac{15}{p_o})^2\frac{1}{L_{rad}} \tag{17}$$

And thus from equation(16) we have

$$\lambda = \frac{\sigma_\theta^2}{L} \tag{18}$$

Scattering density therefore expresses the mean square of the scattering distributions expected for muons with nominal momentum passing through a unit depth of a material with radiation length $L_{rad}$. In Tables(1,2,3,4) we list the values of the radiation lengths of three different classes of elements used in this study. In the following, we present our results of the scattering densities for 20 different elements at different values of momenta of the muons(1,3,4 and 10 GeV). The results for low-Z materials are presented in Fig.1. For medium-Z materials our results are presented in Fig 2 and finally for the case of high-Z materials our results are plotted in Fig.3.

### 3.1.1 Scattering density of three different classes of elements at momentum 1GeV

In Table(1), we present our results for evaluation of the standard deviation $\sigma$ and scattering density $\lambda$ of three different classes of elements based on their atomic number Z at momentum equal ($1GeV$) using radiation length as an input parameter. Note that the scattering density is very small for gases compared to other materials.The large values of scattering densities in solids is due to the small distance between the nuclei of their atoms, which causes an increase in attraction and repulsion between the muons and nuclei of the atoms.

Table 1: Scattering densities of three different classes of elements at momentum equal $1GeV$.,where G:Gas,L:Liquid and S:Solid.

| 1-Low-Z Material | | | | | | |
|---|---|---|---|---|---|---|
| Z | Material | Symbol | State | $L_{rad}(cm)$ | $\sigma(mrad^2)$ | $\lambda(mrad^2/cm)$ |
| 1 | Hydrogen | H | G | 752300 | 0.0546885 | 0.000299083 |
| 2 | Helium | He | G | 560000 | 0.0633866 | 0.000401786 |
| 3 | Lithium | Li | S | 155 | 3.81 | 1.45161 |
| 4 | Beryllium | Be | S | 35.3 | 7.98369 | 6.37394 |
| 6 | Carbon | C | S | 18.8 | 10.9399 | 11.9681 |
| 7 | Nitrogen | N | G | 33100 | 0.260722 | 0.00679758 |
| 8 | Oxygen | O | G | 25800 | 0.295312 | 0.00872093 |
| 10 | Neon | Ne | G | 24.0 | 9.68246 | 9.375 |
| 13 | Aluminum | Al | S | 8.9 | 15.9 | 25.2809 |
| 14 | Silicon | Si | S | 9.36 | 15.5043 | 24.0385 |
| 18 | Argon | Ar | G | 14.0 | 12.6773 | 16.0714 |
| 2-Medium-Z Material | | | | | | |
| 26 | Iron | Fe | S | 1.76 | 35.7548 | 127.841 |
| 29 | Copper | Cu | S | 1.43 | 39.6664 | 157.343 |
| 35 | Bromine | Br | L | 3.71 | 24.6266 | 60.6469 |
| 47 | Silver | Ag | S | 0.86 | 51.1496 | 261.628 |
| 53 | Iodine | I | S | 1.74 | 35.9597 | 129.31 |
| 3-High-Z Material | | | | | | |
| 74 | Tungsten | W | S | 0.35 | 80.1784 | 642.857 |
| 79 | Gold | Au | S | 0.3344 | 82.0272 | 672.847 |
| 82 | Lead | Pb | S | 0.56 | 63.3866 | 401.786 |
| 92 | Uranium | U | S | 0.3166 | 84.3016 | 710.676 |

### 3.1.2 Scattering density of three different classes of elements at momentum 3GeV

In Table(2), we present our results for evaluation of the standard deviation $\sigma$ and scattering densities $\lambda$ at momentum equal ($3GeV$). We observe similar results to the previous case. It is possible to distinguish between different materials through the different ranges of the scattering densities where ( low-Z materials have $\lambda \leq 5$, medium-Z materials have $5 < \lambda \leq 30$ and high-Z materials have $\lambda \geq 30$)[9].

Table 2: Scattering densities of three different classes of elements at momentum equal $3GeV$.

| 1-Low-Z Material | | | | | | |
|---|---|---|---|---|---|---|
| Z | Material | Symbol | State | $L_{rad}(cm)$ | $\sigma(mrad^2)$ | $\lambda(mrad^2/cm)$ |
| 1 | Hydrogen | H | G | 752300 | 0.0182295 | 0.0000332314 |
| 2 | Helium | He | G | 560000 | 0.0211289 | 0.0000446429 |
| 3 | Lithium | Li | S | 155 | 1.27 | 0.16129 |
| 4 | Beryllium | Be | S | 35.3 | 2.66123 | 0.708215 |
| 6 | Carbon | C | S | 18.8 | 3.64662 | 1.32979 |
| 7 | Nitrogen | N | G | 33100 | 0.0869072 | 0.000755287 |
| 8 | Oxygen | O | G | 25800 | 0.0984374 | 0.000968992 |
| 10 | Neon | Ne | G | 24.0 | 3.22749 | 1.04167 |
| 13 | Aluminum | Al | S | 8.9 | 5.29999 | 2.80899 |
| 14 | Silicon | Si | S | 9.36 | 5.16811 | 2.67094 |
| 18 | Argon | Ar | G | 14.0 | 4.22577 | 1.78571 |
| 2-Medium-Z Material | | | | | | |
| 26 | Iron | Fe | S | 1.76 | 11.9183 | 14.2045 |
| 29 | Copper | Cu | S | 1.43 | 13.2221 | 17.4825 |
| 35 | Bromine | Br | L | 3.71 | 8.20886 | 6.73854 |
| 47 | Silver | Ag | S | 0.86 | 17.0499 | 29.0698 |
| 53 | Iodine | I | S | 1.74 | 11.9866 | 14.3678 |
| 3-High-Z Material | | | | | | |
| 74 | Tungsten | W | S | 0.35 | 26.7261 | 71.4286 |
| 79 | Gold | Au | S | 0.3344 | 27.3424 | 74.7608 |
| 82 | Lead | Pb | S | 0.56 | 21.1289 | 44.6429 |
| 92 | Uranium | U | S | 0.3166 | 28.1005 | 78.964 |

### 3.1.3 Scattering density of three different classes of elements at momentum 4GeV

In Table(3), we present our results for evaluation of the standard deviation $\sigma$ and scattering density $\lambda$ at momentum equal ($4GeV$).

### 3.1.4 Scattering density of three different classes of elements at momentum 10GeV

In Table(4), we present our results for evaluation of the standard deviation and scattering densities at momentum equal ($10GeV$). Note that scattering densities of gas state materials are very small compared to other materials. This can be explained as the nuclei of atoms of gaseous materials have a small effect on the muons passing between them due to the large distances between these atoms, compared with solid and liquid materials. The decrease in the scattering densities in materials can be explained as the increasing of muons momenta leads to a decrease in attraction and repulsion between the muons and nuclei of the atoms.

In Figures (1, 2, 3), we show our results of scattering densities of low-Z,medium-Z, and high-Z materials at different momenta. We note from the figures that, at the momenta of muon 1 GeV and 3 GeV gases with small atomic numbers do not appear as they have small

Table 3: Scattering densities of three different classes of elements at momentum equal $4GeV$.

| 1-Low-Z Material | | | | | | |
|---|---|---|---|---|---|---|
| Z | Material | Symbol | State | $L_{rad}(cm)$ | $\sigma(mrad^2)$ | $\lambda(mrad^2/cm)$ |
| 1 | Hydrogen | H | G | 752300 | 0.0136721 | 0.0000186927 |
| 2 | Helium | He | G | 560000 | 0.0158466 | 0.0000251116 |
| 3 | Lithium | Li | S | 155 | 0.952501 | 0.0907258 |
| 4 | Beryllium | Be | S | 35.3 | 1.99592 | 0.398371 |
| 6 | Carbon | C | S | 18.8 | 2.73497 | 0.748005 |
| 7 | Nitrogen | N | G | 33100 | 0.0651804 | 0.000424849 |
| 8 | Oxygen | O | G | 25800 | 0.0738281 | 0.000545058 |
| 10 | Neon | Ne | G | 24.0 | 2.42061 | 0.585938 |
| 13 | Aluminum | Al | S | 8.9 | 3.97499 | 1.58006 |
| 14 | Silicon | Si | S | 9.36 | 3.87609 | 1.5024 |
| 18 | Argon | Ar | G | 14.0 | 3.16933 | 1.00446 |
| 2-Medium-Z Material | | | | | | |
| 26 | Iron | Fe | S | 1.76 | 8.93871 | 7.99006 |
| 29 | Copper | Cu | S | 1.43 | 9.91661 | 9.83392 |
| 35 | Bromine | Br | L | 3.71 | 6.15665 | 3.79043 |
| 47 | Silver | Ag | S | 0.86 | 12.7874 | 16.3517 |
| 53 | Iodine | I | S | 1.74 | 8.98994 | 8.0819 |
| 3-High-Z Material | | | | | | |
| 74 | Tungsten | W | S | 0.35 | 20.0446 | 40.1786 |
| 79 | Gold | Au | S | 0.3344 | 20.5068 | 42.0529 |
| 82 | Lead | Pb | S | 0.56 | 15.8466 | 25.1116 |
| 92 | Uranium | U | S | 0.3166 | 21.0754 | 44.4172 |

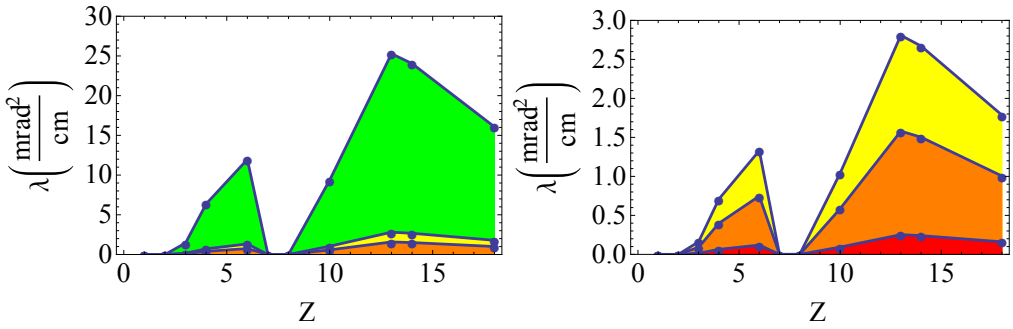


Figure 1: Scattering densities of low-Z materials. In the left, green, yellow and orange colors correspond to muon momenta 1, 3 and 4 GeV respectively. In the right, yellow, orange and red colors correspond to muon momenta 3, 4 and 10 GeV respectively.

values of the scattering densities, while other materials can be distinguished according to their scattering densities. We also note that the scattering density of tungsten is greater than that of lead although lead has a larger atomic number than that of tungsten. This is because the density of tungsten is larger than the density of lead. At the momentum of

Table 4: Scattering densities of three different classes of elements at momentum equal $10GeV$.

| 1-Low-Z Material | | | | | | |
|---|---|---|---|---|---|---|
| Z | Material | Symbol | State | $L_{rad}(cm)$ | $\sigma(mrad^2)$ | $\lambda(mrad^2/cm)$ |
| 1 | Hydrogen | H | G | 752300 | 0.00546885 | 0.00002990830 |
| 2 | Helium | He | G | 560000 | 0.00633866 | 0.00004017860 |
| 3 | Lithium | Li | S | 155 | 0.381 | 0.0145161 |
| 4 | Beryllium | Be | S | 35.3 | 0.798369 | 0.0637394 |
| 6 | Carbon | C | S | 18.8 | 1.09399 | 0.119681 |
| 7 | Nitrogen | N | G | 33100 | 0.0260722 | 0.0000679758 |
| 8 | Oxygen | O | G | 25800 | 0.0295312 | 0.0000872093 |
| 10 | Neon | Ne | G | 24.0 | 0.968246 | 0.09375 |
| 13 | Aluminum | Al | S | 8.9 | 1.59 | 0.252809 |
| 14 | Silicon | Si | S | 9.36 | 1.55043 | 0.240385 |
| 18 | Argon | Ar | G | 14.0 | 1.26773 | 0.160714 |
| 2-Medium-Z Material | | | | | | |
| 26 | Iron | Fe | S | 1.76 | 3.57548 | 1.27841 |
| 29 | Copper | Cu | S | 1.43 | 3.96664 | 1.57343 |
| 35 | Bromine | Br | L | 3.71 | 2.46266 | 0.606469 |
| 47 | Silver | Ag | S | 0.86 | 5.11496 | 2.61628 |
| 53 | Iodine | I | S | 1.74 | 3.59597 | 1.2931 |
| 3-High-Z Material | | | | | | |
| 74 | Tungsten | W | S | 0.35 | 8.01784 | 6.42857 |
| 79 | Gold | Au | S | 0.3344 | 8.2027 | 6.72847 |
| 82 | Lead | Pb | S | 0.56 | 6.3386 | 4.01786 |
| 92 | Uranium | U | S | 0.3166 | 8.43016 | 7.10676 |

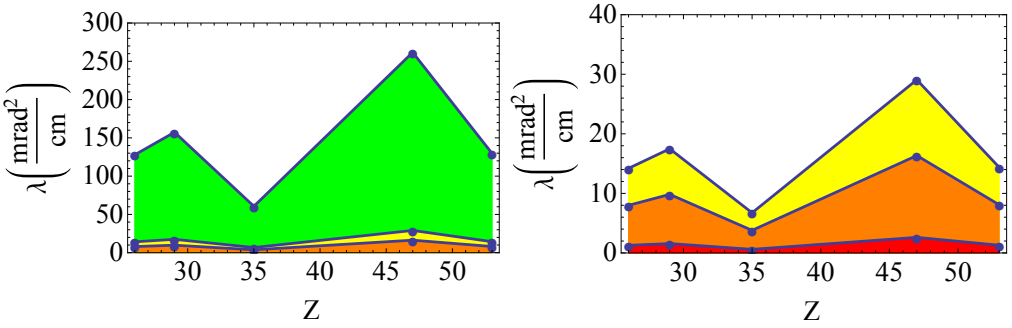


Figure 2: Scattering densities of medium-Z materials. In the left, green, yellow and orange colors correspond to muon momenta 1, 3 and 4 GeV respectively. In the right, yellow, orange and red colors correspond to muon momenta 3, 4 and 10 GeV respectively.

muon 4 GeV, we observe the same results but the only difference is that, the scattering density value of each material decrease with increasing the momentum of the muons. At the momentum of muon 10 GeV, we notice from the figures that there is a decrease in

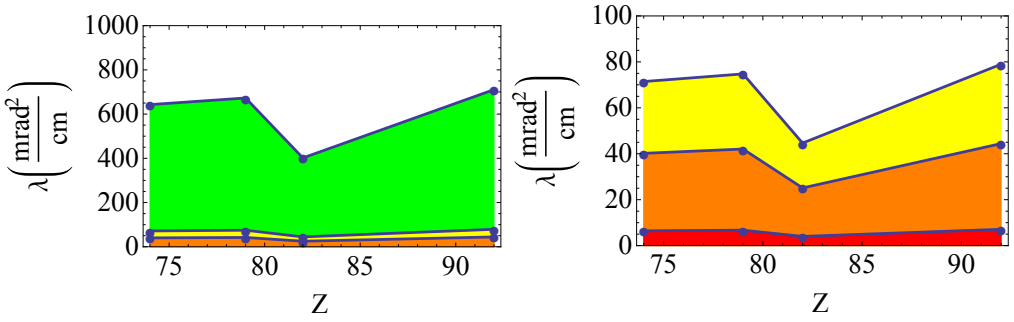


Figure 3: Scattering densities of high-Z materials. In the left, green, yellow and orange colors correspond to muon momenta 1, 3 and 4 GeV respectively. In the right, yellow, orange and red colors correspond to muon momenta 3, 4 and 10 GeV respectively.

the scattering density value of each material with increasing the momentum of the muons as in the previous cases. Note that scattering densities of gaseous state materials are very small compared to other materials. This can be explained as the nuclei of atoms of gaseous materials have a small effect on the muons passing between them due to the large distances between these atoms, compared with solid and liquid materials. In all figures, the decrease in the scattering densities with increasing muon momenta, for all materials, can be explained as increasing the muons momenta leads to a decrease in attraction and repulsion between the muons and nuclei of the atoms.

Finally the results of this study is based on Moliere's interpretations of the charged particles with matter [10, 11] and the study done in the laboratory of Los Alamos National Laboratory (LANL) in which only three different materials (iron - concrete - uranium) were studied at the muon energies(3 - 4) GeV [7, 9]. It should be note that in this study we consider 20 different materials for the range of muon energies ( 1 - 3 - 4 - 10) GeV.

## 4 CONCLUSIONS

Muography as an imaging technique is based on the absorption or scattering of atmospheric muons produced from cosmic-ray interactions in the atmosphere. This technique has the ability to investigate the interior of natural or artificial structures and can help, for instances, to make a surveys on nuclear wastes, homeland security, monitoring of natural hazard such as volcanic eruptions and material identifications. When muons pass through material they produce aggregate of scattering angles with an approximate Gaussian distribution. Theoretically, the standard deviation of the distribution can be calculated using the radiation length of the substance. Since scattering density depends on the standard deviation of the distribution, we therefore have provided our results for the scattering densities of 20 elements ranging from low, medium and high Z number. For these 20 elements, we calculated their scattering densities at different four values of the momentum of the muons, namely at momenta (1, 3, 4 and 10 GeV) to show its dependency on the momentum. This technique has the ability to break through the big thickness of materials in the comparison with another technique as example x-ray, without causing any damage to the inspected materials. As demonstrated in previous studies, where it has been shown to be effective in detecting substances, references can be reviewed at [2, 7, 21, 22]

## Conflict of Interest Declaration

The authors declare that there is no conflict of interest statement.

## Ethics Committee Approval and Informed Consent

The authors declare that there is no ethics committee approval and/or informed consent statement.

## References

[1] A. Bettini, Introduction to Elementary Particle Physics, Cambridge University Press, Cambridge, 2008.

[2] S. Procureur, Muon imaging Principles, technologies and applications, Nucl. Instrum. Methods Phys. Res A., 878 2018, 169-179.

[3] P. K. F. Grieder, Cosmic Ray at Earth Researcher's Reference and Data Book, Elsevier, Amsterdam, 2001.

[4] K. Nagamine. Introductory Muon Science. Cambridge University Press, Cambridge, 2003.

[5] E.P. George. Cosmic rays to inspect large volumes. Commonwealth Engineer, 1955, 455-457.

[6] L. W. Alvarez, J.A. Anderson, F.E. Bedwei, J. Burkhard, A. Fakhry, A. Girgis, A. Goneid, F. Hassan, D. Iverson, G. Lynch, et al. Search for hidden chambers in the pyramids. Science New York, 167(3919) 1970, 832.

[7] Marilena Bandieramonte, Muon Portal project: Tracks reconstruction, automated object recognition and visualization techniques for muon tomography data analysis, IEEE International Conference on Technologies for Homeland Security, 2015, 517-522.

[8] M. Gupta, Calculation of radiation length in materials,PH-EP-Tech-Note, 2010-013.

[9] L. J. Schultz, K.N.Borozdin, J.J. Gomez, G.E.Hogan, J.A. McGill, C.L. Morris, W. C. Priedhorsky, A. Saunders, M.E.Teasdale, Image reconstruction and material Z discrimination via cosmic ray muon radiography, Nucl. Instrum. Methods Phys. Res A, 519 2004, 687-694.

[10] Scott. WT, the theory of small-angle multiple scattering of fast charged particles, Reviews of modern physics,1963, volume 35 pages231.

[11] H. A. Bethe, Moliere's theory of multiple scattering, Phys. Rev., 89 1953, 1256.

[12] P. La Rocca, V. Antonuccio, M. Bandieramonte, U. Becciani, F. Belluomo, M. Belluso, S. Billotta, A. A. Blancato, D. Bonanno, G. Bonanno, Search for hidden high-Z materials inside containers with the Muon Portal Project,J. Instrum., 9 2014, C01056.

[13] L. Cremonesi, Cosmic ray muon tomography for anti-terrorism applications, Master Thesis, University College of London, 2011.

[14] G. R. Lynch and O. I. Dahl, Approximations to multiple coulumb scattering, Nucl. Instrum. Methods Phys. Res B, 58 1991, 6-10.

[15] S. I. Dutta, M. H. Reno, I. Sarcevic, and D. Seckel, Propagation of muons and taus at high energies, Phys. Rev. D, 63 2001, 094020.

[16] K. N. Borozdin, G. E. Hogan, C. M., W. C. Priedhorsky, A. Saunders, L. J. Schultz, M. E. Teasdale, Radiographic Imaging with Cosmic Ray Muons, Nature 422 2003, 277.

[17] B. Schwarzschild, Cosmic-ray muons might help thwart transport of concealed fissile material, Physics Today, 56(5) 2003, 19-22.

[18] National Public Radio,Detecting Nuclear Smugglers, All Things Considered radio broadcast,June 13, 2003.

[19] J. Roach, Cosmic Particles could Detect Nuke Materials, National Geographic News, 2003.

[20] P. Weiss, Muon Manna? Particle Shower may Spotlight Loose Nukes, Science News Online, 163 2003, 179.

[21] L. Olah, Research and development of particle detectors for muon tomography and the CERN ALICE experiment, PhD Thesis, Budapest, 2016.

[22] N. Lesparre, D. Gilbert, Y. Marteau, Y. Declais, D. Carbone and E. Galicet, Geophysical muon imaging: feasibility and limits, Geophys. J. Int. 183(3), (2010), 1348-1361.